Journal of Power Sources 196 (2011) 6305–6317

Contents lists available at ScienceDirect

Journal of Power Sources

journal homepage: www.elsevier.com/locate/jpowsour

Water balance simulations of a polymer-electrolyte membrane fuel cell using a two-fluid model

T. Berning[a,*], M. Odgaard[b], S.K. Kær[a]

[a] Department of Energy Technology, Aalborg University, 9220 Aalborg, Denmark
[b] IRD A/S, 5700 Svendborg, Denmark

ARTICLE INFO

Article history:
Received 12 January 2011
Received in revised form 2 March 2011
Accepted 27 March 2011
Available online 6 April 2011

Keywords:
PEM fuel cells
Water balance
CFD modeling
Multi-phase modeling
Micro-porous layer
Water-uptake layer

ABSTRACT

A previously published computational multi-phase model of a polymer-electrolyte membrane fuel cell cathode has been extended in order to account for the anode side and the electrolyte membrane. The model has been applied to study the water balance of a fuel cell during operation under various humidification conditions. It was found that the specific surface area of the electrolyte in the catalyst layers close to the membrane is of critical importance for the overall water balance. Applying a high specific electrolyte surface area close to the membrane (a *water-uptake layer)* can prevent drying out of the anode and flooding at the cathode while the average membrane water content is only weakly affected. The results also indicate that in contrast to common presumption membrane dehydration may occur at either anode or cathode side, entirely depending on the direction of the net water transport because the predominant transport mechanism is diffusion. Consequently, operating conditions with a high net water transport from anode to cathode should be avoided as it is important to keep the cathode catalyst layer well humidified in order to prevent high protonic losses. Addition of the micro-porous layer did not affect the overall water balance or membrane water content in our study.

1. Introduction

A fundamental understanding of the water balance of a fuel cell during operation is crucial for improving the cell performance and durability. It is well known that an improper water management will lead to excessive flooding of the cathode and presumably to drying out of the anode as water is being dragged from anode to cathode along with the protonic flux through the membrane, a process commonly named electro-osmotic drag (EOD). The EOD coefficient has been experimentally determined to be around unity by Zawodzinski et al. [1] and Ye and Wang [2], meaning that one water molecule per proton is dragged from anode to cathode. An EOD of unity already means that twice the amount of product water created at the cathode is dragged from anode to cathode, and the conventional means of providing sufficient water to the anode to prevent drying out is to humidify the incoming anode gas stream [3] and to allow for back diffusion of water from cathode to anode. To this end the diffusivity of water through the membrane has been measured by several research groups (e.g. [4]). Recently, Monroe et al. [5] have conducted experiments on a plane membrane and found that for thin (<50 μm) membranes as they are being used nowadays the overall water transport may not be controlled by diffusion inside the membrane phase, but also by the absorption/desorption kinetics of water to/from the electrolyte phase. Ge et al. [6] have in turn measured that water absorption to the membrane is around one order of magnitude slower than desorption, and their experiments were conducted on the operating fuel cell.

In this work we have extended a previously published model [7,8] in order to account for the anode side and the polymer-electrolyte membrane. Water transport across the membrane is modeled using a constant EOD of unity and a diffusion coefficient of water in the electrolyte phase taken from the literature. The absorption coefficient was also taken from the literature, but in our study the specific surface area of the electrolyte in the catalyst layer to uptake the water was varied over one order of magnitude. It will be shown that this parameter is very important for the overall water balance. We also confirm that for thin membranes the diffusion of water in the electrolyte may not be rate determining.

For the water balance it is desirable that the fuel cell cathode does not become flooded and the anode does not become dry. In addition, the water content λ of the electrolyte membrane should be as high as possible in order to reduce ohmic losses. A layer with a high specific surface area α of the electrolyte to facilitate sufficiently fast water absorption is called a *water-uptake layer* in our work, and it is found that such a layer may substantially increase

* Corresponding author at: Department of Energy Technology, Aalborg University, Pontoppidanstraede 101, 9220 Aalborg, Denmark. Tel.: +45 9940 9261; fax: +45 98151411.
E-mail address: tbe@et.aau.dk (T. Berning).

0378-7753/$ – see front matter © 2011 Elsevier B.V. All rights reserved.
doi:10.1016/j.jpowsour.2011.03.068

Nomenclature

a	water activity
C	mass concentration ($kg\,m^{-3}$)
D	diffusion coefficient ($m^2\,s^{-1}$)
EW	equivalent weight of dry membrane (=1.1 $kg\,mol^{-1}$)
F	Faraday's constant (=96,485 $C\,mol^{-1}$)
f_v	specific volume fraction of water in the membrane
f_l	specific volume fraction of water in the liquid-equilibrated membrane
i''	current density ($A\,cm^{-2}$)
K	permeability (m^2)
k_a, k_d	kinetic absorption/desorption coefficient ($m\,s^{-1}$)
k_{rel}	relative permeability
M	molecular weight ($kg\,mol^{-1}$)
n_d	drag coefficient
P	pressure (Pa)
S	source term
s	saturation
r_{drag}	effective (net) drag coefficient
T	temperature (K)
$\mathbf{U}$	velocity vector $\mathbf{U}=(u, v, w)$
V_m	partial molar volume of dry membrane
V_w	partial molar volume of membrane water
Y	dimensionless mass fraction

Greek symbols

α	specific electrolyte surface area ($m^2\,m^{-3}$)
ε	porosity
θ	contact angle
λ	membrane water content
ν	molecular viscosity ($m^2\,s^{-1}$)
μ	dynamic viscosity ($kg\,m^{-1}\,s^{-1}$)
ρ	density ($kg\,m^{-3}$)
ρ^{mem}	dry membrane density (=2000 $kg\,m^{-3}$)
Γ	product of density and diffusion coefficient

Subscripts

a	absorption
d	desorption
equil	equilibrium value
w	(membrane) water

Superscripts

mem	membrane

Abbreviations

BP	bipolar plate
CL	catalyst layer
CFD	computational fluid dynamics
EOD	electro-osmotic drag
GDL	gas diffusion layer
MEA	membrane electrode assembly
MPL	micro-porous layer
PEMFC	polymer electrolyte membrane fuel cell
RH	relative humidity

the limiting current density when operating the cell under dry inlet conditions. In practice, such a layer can be applied by increasing the mass fraction of electrolyte phase inside the CL in the vicinity of the membrane as an integral part of a multi-layer electrode [9].

2. Literature review

There are a number of publications on water balance in a fuel cell employing both experimental and numerical methods. An overview of water balance issues and experimental efforts was given by Dai et al. [10], and Baschuk and Li gave a summary of ion and water transport phenomena in membranes [11].

Theoretical studies employed either analytical models (e.g. [4,12,13]) or the methods of computational fluid dynamics (CFD) (e.g. [14]). While publications of CFD models for PEMFC abound in the literature [15] there are only few detailed studies published on the water balance during operation. This is particularly unfortunate because water balance is one of the few non-intrusive experiments that can be reliably conducted and thus used for model validation. Luo et al. [16] presented probably the most detailed fuel cell CFD model to date, but did not publish a detailed study on water balance in a PEMFC. The study published by Lee et al. [14] was based on the commercial fuel cell module by CD Adapco, which is essentially single phase and contains only a simplified membrane model. Both models do not account for the sorption/desorption kinetics of water into and out of the electrolyte phase but instead assume equilibrium between the electrolyte phase and the adjacent gas phase in terms of water content. Wu et al. [17] and Ye and Nguyen [18] published CFD modeling studies that accounted for the sorption/desorption kinetics but assumed constant proportionality values and did not investigate the effect of the kinetics and specific surface area of the electrolyte. Liu et al. [19] conducted experiments using a 30 μm Gore membrane and obtained a distributed net drag coefficient via postprocessing. The calculated net drag was low and even negative due to strong back diffusion. Finally, Wu et al. [17] published a three-dimensional multi-phase CFD model that accounted for membrane water transport and included sorption and desorption terms. Unfortunately, they did not publish a detailed water balance study either.

Experimental work on water transport across the membrane was reported by Janssen and Overvelde [20], Cai et al. [21] and Karan et al. [22], among others. Janssen and Overvelde applied various humidification conditions at both anode and cathode side corresponding to either fully saturated or entirely dry gases. The resulting effective drag coefficient was positive (water transport from anode to cathode) for most cases. However, experiments conducted on a Nafion 122 membrane (50 μm thickness) also show that the net drag can be negative for such thin membranes under fully humidified conditions [20].

Karan et al. [22] performed experiments with an (inlet-) RH gradient between anode and cathode and found that the drag coefficient was positive for the cases investigated (A/C 100%/60% and 60%/100% with and without MPL, respectively). Yan et al. [23] took water balance data at various operating conditions and found that depending on the RH of the feed gases the net drag could be either positive or negative. Ye and Wang [24] measured a positive drag coefficient over a wide range of operating conditions. Overall it can be stated that experiments were published only for a few, chosen operating and material conditions.

It is important to realize that most of above studies were conducted using relatively low stoichiometric flow ratios of 2–3. While this provides a better match with realistic fuel cell operating conditions it is bound to yield three-dimensional effects in any given set-up. Consequently the local net drag will vary from inlet to outlet and depend on co- and counter flow conditions. The measured lump value for the net drag is an integral value of the local values, which makes these data difficult to compare. While above experiments provided information about net water transport under realistic operating conditions they are not very suitable for improving the fundamental understanding.

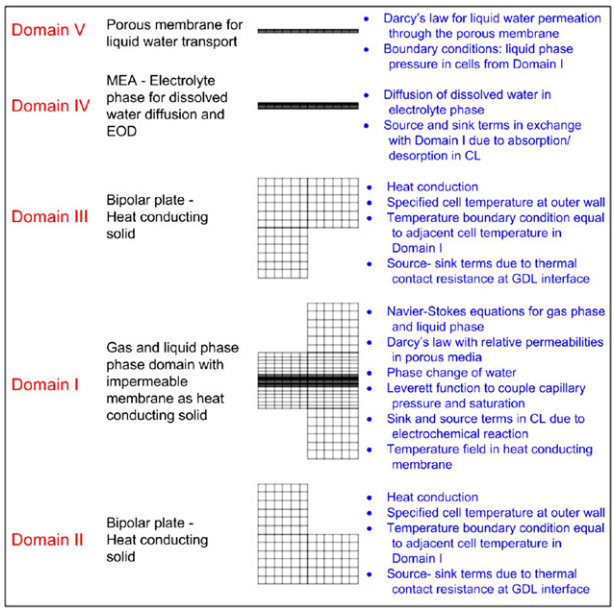

Fig. 1. Two-dimensional cut through the computational domains and summary of physical models applied [46].

Ideally, water balance measurements should be conducted at a high stoichiometric flow ratio in order to limit the problem to be two-dimensional (no down-the-channel variation). If in addition the channel-rib spacing is chosen very fine we are left with a quasi one-dimensional problem which will proof to be complex enough for water balance studies. Experiments conducted in the three-dimensional mode are of limited value for model validation purposes because of the large number of material parameters and uncertainties involved.

While detailed experiments on water balance can be very costly, a simulation with this model took approximately 2 h per data point on a laptop computer with 2.2 GHz, which allowed for a very detailed case study. The drawback is that no CFD model of a fuel cell has been extensively validated. Models are currently being used to shed additional insight into experiments conducted and can also be used to suggest new experiments that verify some of the modeling findings.

3. Model description

The model is based on the formerly commercial CFD package CFX-4.4 (ANSYS Inc.). The advantage of this code is the implementation of a multi-fluid model and the possibility to customize the code via an extensive suite of FORTRAN user subroutines. In this section we will give a description of the physical model. Fig. 1 shows a two-dimensional y–z-cut of our computational domains. The x-direction is defined as the down-the-channel direction.

It can be seen that we have utilized five separate computational domains to model the various transport processes that occur in a fuel cell. These domains communicate with each other via implemented source and sink terms as will be described below. It is important to realize that *Domain IV* is an exact copy of the membrane-electrode assembly (MEA) cells from *Domain I* so that there is a direct cell-to-cell correspondence. Likewise *Domain V*, which consists of the membrane only, is an exact copy of the membrane from *Domain I*, but while the membrane in *Domain I* is represented by a non-permeable heat-conducting solid, *Domain V* is a porous region where the Darcian transport of liquid water through the membrane is modeled with appropriate pressure boundary conditions and employing a local hydraulic permeability that is a function of the membrane water content calculated in *Domain IV*. More details of the purposes and equations applied in the different computational domains are given below.

3.1. Domain I

This is the main computational domain where we solve for the gas phase and liquid phase flow in the channels and porous media: the gas diffusion layer (GDL), micro-porous layer (MPL) – if included – and the catalyst layer (CL). For each thermodynamic phase a complete set of Navier–Stokes equations (plus energy equation) is solved. In addition species conservation equations for oxygen and water vapor at the cathode side and hydrogen and water vapor at the anode side are solved. Phase change of water is accounted for at both anode and cathode side. Boundary conditions are prescribed at the channel inlets in terms of gas composition and temperature (no liquid enters here), while we specify pressure boundary conditions at the outlet. In the porous media the momentum equations reduce to Darcy's law with a different relative permeability of each phase. The liquid phase is transported here by capillary forces and the capillary pressure versus liquid saturation is specified using the Leverett equation [25,26] but only applied to the reducible saturation and thus allowing for simulating a porous medium with a mixed wettability (hydrophilic and hydrophobic pores). In our model a different irreducible saturation can be specified for every layer, for example the catalyst layers contain a much larger fraction of hydrophilic pores than the MPL. We have previously argued that the shape of the Leverett function should be closely related to the integrated pore-size distribution [7] and this could conceivable be captured by adjusting the coefficients in the cubical Leverett equation. Finally, a different effective liquid water contact angle θ can be specified for every porous region. This contact angle applies only for the hydrophobic, water transporting pores. Table 1 lists important material parameters employed in the current study. In our previous study it was found that the irreducible saturation predominantly dictates the saturation level encountered in every layer. Specifying different material properties means that we will encounter a saturation jump between every adjacent layer because the capillary pressure has to be continuous across each interface [27].

Inside the three-dimensional cathode CL there is oxygen consumption and production of liquid water according to a specified local current density that depends on the local oxygen concentration. A detailed electrochemical model is not yet implemented. Along with the water production there is heat production due to an assumed local overpotential as described in reference [7]. To summarize, *Domain I* is utilized to calculate the gas phase and liquid phase flow fields in the gas flow channels and porous media. Anode side and cathode side are separated by an impermeable membrane that only allows for heat conduction. Species equations are solved for oxygen, water vapor and hydrogen while nitrogen is assumed as background fluid. There is no oxygen or nitrogen at the anode and no hydrogen at the cathode. The exchange of water between anode and cathode is calculated in *Domain IV* and *Domain V*.

3.2. Domains II and III

These domains represent the bipolar plates (BPs) and currently they are only used to calculate heat conduction. Consequently the only equation of interest here is the energy equation to yield the temperature distribution inside the bipolar plates. Boundary conditions have been prescribed at the outside walls in form of the desired cell operating temperature. The computational cells adjacent to the flow channels communicate with cells in *Domain I* by applying the temperature in the adjacent flow channel cell as the boundary condition for *Domains II* and *III* and vice versa, which makes for a very robust numerical scheme. A thermal con-

Table 1
Porous material properties applied in the current study.

Region name	Irreducible saturation [−]	Contact angle [°]	Permeability [m^2]	Porosity [−]	Tortuosity [−]
GDL	0.20	120	1.0E−12	0.75	4
MPL	0.10	130	0.1E−12	0.75	6
CL	0.30	110	0.1E−12	0.75	4

tact resistance at the interface between the BP and the GDL has been implemented to account for contact losses. In the future this domain will also be used to calculate the electrical field equation.

3.3. Domain IV

This domain represents the electrolyte phase of the MEA, and it accounts for the transport of water between anode and cathode side. The only equation of interest solved here is the conservation of dissolved water in the electrolyte phase [28]. Thus a pure diffusion equation is solved with source terms inside the CL due to sorption/desorption of water. The electro-osmotic drag coefficient is assumed constant in this work which leads to an additional non-zero source term for the electrolyte water inside the CL. The diffusion coefficient is itself a function of membrane water content and temperature, and it has been taken from the literature [4].

Mathematically the transport equation that is solved here is the standard convection–diffusion equation in CFX-4 [28]:

$$\nabla \cdot (\rho \mathbf{U} Y_w) - \nabla \cdot (\Gamma_w \nabla Y_w) = S \tag{1}$$

where ρ is the density, $\mathbf{U}$ is the bulk velocity vector, Γ_W is the product of density and the diffusion coefficient, Y_W the water mass fraction in the membrane and S is a source term. The convective term (first term) inside the membrane was set to zero as there is no net velocity of the electrolyte phase, which leaves only the diffusion and source term. The mass fraction Y_w can be replaced by the mass concentration C_w divided by the density of the membrane ρ_{mem}. This yields [16]:

$$-\nabla \cdot \left(\rho^{mem} D_W^{mem} \nabla \frac{C_w}{\rho^{mem}} \right) = S \tag{2}$$

Neglecting the swelling of the membrane the density terms can be cancelled against each other. The correlation between the concentration of water and the dimensionless water content λ was given by Springer et al. [4]:

$$C_w = \frac{\rho^{mem}}{\mathrm{EW}} M_W \times \lambda = \left(\frac{2000\ \mathrm{kg\ m^{-3}}}{1100\ \mathrm{kg\ kmol^{-1}}} 18\ \mathrm{kg\ kmol^{-1}} \right) \times \lambda = 32.73\ \mathrm{kg\ m^{-3}} \times \lambda \tag{3}$$

While the dimensionless mass fraction solved for by CFX-4 is that value divided by the membrane density:

$$Y_w = \frac{C_w}{\rho^{mem}} \lambda = 0.016364 \times \lambda \tag{4}$$

This yields for Eq. (2):

$$-\rho^{mem} \frac{M_W}{\mathrm{EW}} \nabla \cdot (D_W^{mem} \nabla \lambda) = S \tag{5}$$

where ρ^{mem} is the density of the dry membrane (2000 kg m^{-3}) and EW its equivalent weight (1100 kg kmol^{-1}). A very similar transport equation is used by Gurau et al. [28]. It must be considered though that CFX-4 can only solve a transport equation in the form of Eq. (1) with the restriction that Y_W is smaller than or equal to unity. For the diffusivity of water inside the membrane $D_{w,mem}$ we used the expression suggested by Springer et al. [4]:

$$D_W^{mem} \times \left[\frac{\mathrm{m^2}}{\mathrm{s}} \right]^{-1} = 10^{-10} \exp\left\{ 2416 \left(\frac{1}{303} - \frac{1}{T} \right) \right\} (2.563 - 0.33\lambda + 0.0264\lambda^2 - 0.000671\lambda^3) \tag{6}$$

By comparison to Eq. (5) Luo et al. [16] solved the following equation in their membrane model:

$$\nabla \cdot \left(\frac{\rho^{mem}}{\mathrm{EW}} D_W^{mem} \nabla \lambda \right) M_W - \nabla \cdot \left(n_d \frac{i''}{F} \right) M_W + \nabla \cdot \left(\frac{K^{mem}}{\nu_l} \nabla p_l \right) = 0 \tag{7}$$

The second term in their equation accounts for the water transport due to electro-osmotic drag. It can be easily shown that for a constant drag coefficient this term is zero inside the membrane and non-zero inside the CL [16,29]. In our model this is accounted for by a source term similar to Gurau et al. [28]:

$$-\frac{\rho^{mem}}{\mathrm{EW}} \nabla \cdot (D_W^{mem} \nabla \lambda) M_W = S_{\lambda(sorp/desorp)} - \nabla \cdot \left(n_d \frac{i''}{F} \right) M_W \tag{8}$$

The third expression in Eq. (7) accounts for liquid phase transport due to convection. In our model this part is treated in *Domain V* (see below). So in contrast to Luo et al. we treat the water dissolved in the membrane phase differently from the water that is permeating through the membrane by pressure forces.

An alternative description of membrane water transport was given by Janssen [30] who published a model for water and protonic transport through the membrane using concentrated solution theory. A similar approach was used by Weber and Newman [31] and Fimrite et al. [32].

The source term due to sorption/desorption of water depends on the sorption kinetics, the specific surface area of the electrolyte inside the CL and a driving force for absorption/desorption due to deviation from the equilibrium value of λ_{equil} (or $C_{w,equil}$) [28]:

$$S_{\lambda(sorp/desorp)} = \alpha \times k_a \times (C_{w,equil} - C_w) \times M_W \tag{9}$$

In case of water absorption to the electrolyte phase there is a source term for the water in the electrolyte phase and a corresponding sink term for the gas phase water in *Domain I*. The specific surface area of the electrolyte phase in the CL, α in [m^2 m^{-3}], is central for the further study. Unfortunately, no detailed data is available in the literature, and we will leave this parameter adjustable. The kinetic sorption coefficient has been determined by Ge et al. [33]:

$$k_a \times \left[\frac{\mathrm{m}}{\mathrm{s}} \right]^{-1} = 1.14 \times 10^{-5}\ f_v \exp\left[2416 \left(\frac{1}{303} - \frac{1}{T} \right) \right] \tag{10}$$

This group also measured the desorption rate to be [33]:

$$k_d \times \left[\frac{\mathrm{m}}{\mathrm{s}} \right]^{-1} = 4.59 \times 10^{-5} f_v \exp\left[2416 \left(\frac{1}{303} - \frac{1}{T} \right) \right] \tag{11}$$

However, in our steady-state model the absorption rate and desorption rate have to coincide in order to prevent the system to become over specified. Hence, the overall process is limited by the sorption rate. The molar water fraction f_v in above equations is taken to be constant at 0.31. This is justifiable considering that the specific surface area is varied over one order of magnitude in this study.

The equilibrium concentration $C_{w,equil}$ was determined by Zawodzinski et al. [34]:

$$C^{mem}_{W,equil} = \frac{\rho^{mem}}{\mathrm{EW}} M_W \times \lambda_{equil} = \frac{\rho^{mem}}{\mathrm{EW}} M_W[(0.043 + 17.81a - 39.85a^2 + 36.0a^3)s_g + 16.8s_l] \quad (12)$$

where a is the activity of water vapor adjacent to the membrane and s_g and s_l are the gas phase and liquid phase saturation (volume fraction), respectively. To summarize, the only transport equation solved in computational *Domain IV* is Eq. (8). It is important to realize that the source terms are non-zero only inside the catalyst layers. In the membrane the right hand side is zero and dissolved water transport reduces the diffusive transport without a source term.

Of note is also that there is an enthalpy term associated with the sorption/desorption of water into and out of the electrolyte phase, although this term has often been neglected in computational fuel cell models. Sorption of water vapor into the electrolyte is similar to condensation, while desorption is similar to evaporation, thus if the overall drag is positive, i.e. from anode to cathode, we have a heating term at the anode and a cooling term at the cathode. The heat of absorption and desorption has been experimentally determined to be very close to the heat of condensation/evaporation of water [35]. This energy source/sink term is accounted for in *Domain I*. One fundamental difference between the water diffusing through the MEA in *Domain IV* and the convection term calculated in *Domain V* is the enthalpy of phase change which is not accounted for when the liquid water is merely pressed through the membrane by the liquid phase pressure gradient between cathode and anode. This model is hence also fundamentally different from the approach used by Eikerling et al. [36] who considered EOD and hydraulic permeation inside the membrane due to capillary pressure forces.

3.4. Domain V

This domain accounts for the hydraulic permeation of water through the membrane. The membrane is considered a porous medium and the liquid phase pressure difference between cathode and anode side drives the water through the water-filled pores in the membrane [37]. Consequently, the only equation of interest is the three-dimensional momentum equation for the liquid phase:

$$\nabla \cdot \varepsilon(\rho_l \mathbf{U}_l \otimes \mathbf{U}_l - \mu_l(\nabla \mathbf{U}_l + (\nabla \mathbf{U}_l)^T)) = \varepsilon \left(\frac{\mu_l}{\varepsilon k_{rel} K_{sat}} \mathbf{U}_l - \nabla p_l \right) \quad (13)$$

As was discussed in our previous work [7] for small bulk velocities $\mathbf{U}_l$ the left hand side of the equation becomes negligible and the right hand side reduces to Darcy's law. The computational domain consists of the membrane only, where again there is a one-to-one correspondence between these computational cells and the membrane computational cells in *Domain I*. Boundary conditions are prescribed in form of two pressure boundaries, where the specified pressures correspond to the liquid phase pressure in the membrane adjacent CL cells from *Domain I*. The permeability of the membrane is a function of the membrane water content calculated in *Domain IV*:

$$k_{rel} K_{sat} = \left(\frac{f_v}{f_L} \right)^2 K_{sat} \quad (14)$$

where K_{sat} is the liquid saturated permeability ($=1.8 \times 10^{-18}\,\mathrm{m}^2$) [38]. The first part is the relative permeability and it depends on the local wetting status of the membrane λ according to [37]:

$$f_v = \frac{\lambda V_w}{V_m + \lambda V_w} \quad (15)$$

The partial molar volume of the dry membrane is defined as:

$$V_m = \frac{\mathrm{EW}}{\rho^{mem}} \quad (16)$$

The partial molar volume of water is simply:

$$V_w = \frac{M_{H_2O}}{\rho_l} \quad (17)$$

where M_{H_2O} is the molecular weight of water ($18\,\mathrm{kg\,kmol^{-1}}$) and ρ_l is the water density ($974\,\mathrm{kg\,m^{-3}}$). The local water content λ is taken from the corresponding control volume in *Domain IV*.

The pressure boundary conditions applied here result in a calculated flux, and this flux in turn is implemented as source/sink term for liquid water in the CL cells adjacent to the membrane in computational *Domain I*. Note that in all cases investigated here the convective water flux was at least two orders of magnitude lower than the fluxes calculated in *Domain IV* and could have been neglected. However, this part of the model was kept for the sake of completeness and because in the future it will allow us to investigate the water flux when a pressure difference between anode and cathode side is applied.

4. Model results

The model was applied to study the water balance for a fuel cell under specified operating conditions. The operating temperature was 80 °C in every case investigated and the outlet pressure was fixed at 1.5 atm. In stoichiometric flow ratio was set to 10 in order to keep the study at a quasi two-dimensional level and simplify postprocessing. It should be stressed that the model is three-dimensional in nature without any numerical restrictions. For this particular study the predicted water balance was investigated for five different cases. Case 1 employed an inlet relative humidity of 100% at both anode and cathode side, Case 2 an inlet RH of 50%/50% and Case 3 was conducted for entirely dry (0% RH) inlet conditions. Cases 4 and 5 were conducted for relative inlet humidities of 0%/100% C/A and 100%/0% C/A, respectively.

4.1. General remarks

This study was conducted in order to shed additional light into the transfer mechanisms of water across the membrane for a fuel cell during operation. A key output parameter is the effective drag of water across the membrane, typically defined as (e.g. [20]):

$$r_{drag} = \frac{n^{in}_{w\_an} - n^{out}_{w\_an}}{j'' \times A/F} \quad (18)$$

where $n_{w\_an,in}$ denotes the incoming molar water stream at the anode and $n_{w\_an,out}$ the outcoming molar stream of water at the anode in [mol s^{-1}]. The difference is of course the net amount of water transferred across the membrane. This amount is normalized by a half amount of water produced, where j'' denotes the nominal current density of the operating cell in [A cm^{-2}], A is its geometrical area in [m^2] and F is the Faraday constant (96,485 C mol^{-1}). A positive effective drag coefficient means that we have net water transport from anode to cathode, and a negative effective drag coefficient means that we have back transport from cathode to anode. In the latter case the back diffusion outweighs the EOD. In our study we generally employed an EOD coefficient of unity, so that a resulting effective drag coefficient of unity means that there is no net back diffusion. In this study we can neglect convective transport of water due to the low pressure difference employed so that we reduce the overall water transport to two phenomena: EOD and back diffusion. As for diffusion it can be said that the diffusivity depends on the water content of the membrane: the larger the water content λ

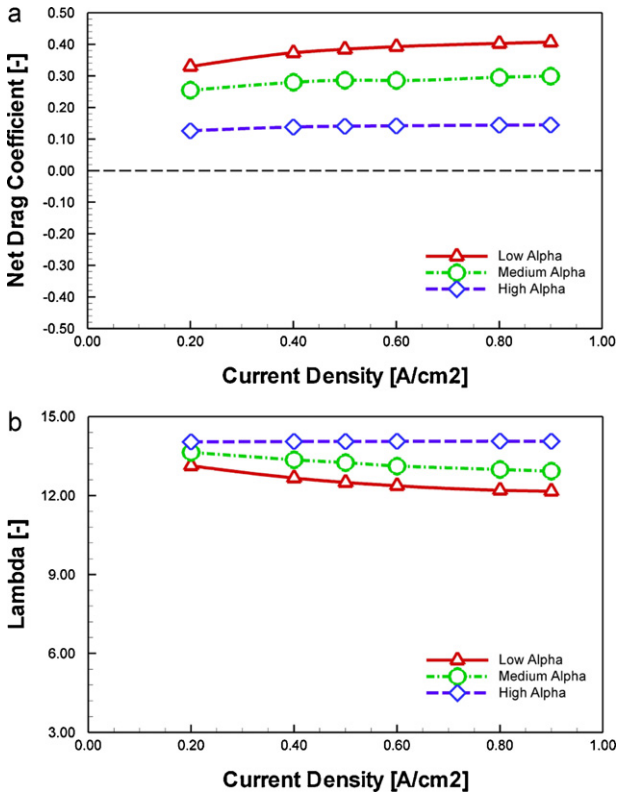

Fig. 2. (a) Predicted net drag coefficient for Case 1 as function of the specific electrolyte surface area α [46]. (b) Predicted average membrane water content λ for Case 1 as function of the specific electrolyte surface area α [46].

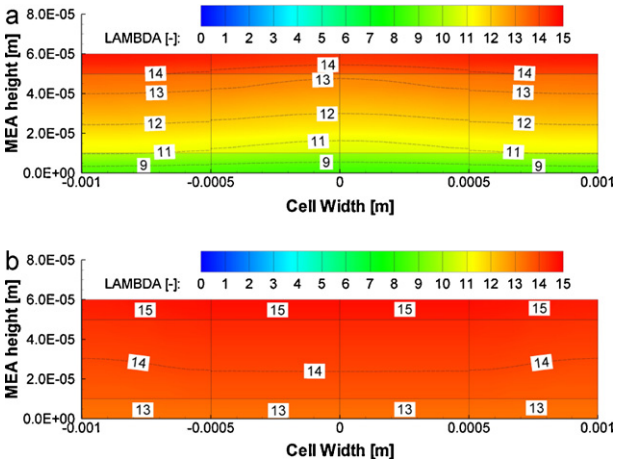

Fig. 3. (a) Predicted MEA water content λ for Case 1 at a current density of 0.8 A cm^{-2} and for a low specific electrolyte surface area $\alpha = 5.0 \times 10^4$ m^2 m^{-3}. The cathode CL is the lower part and the anode CL the upper [46]. (b) Predicted MEA water content λ for Case 1 at a current density of 0.8 A cm^{-2} and for a high specific electrolyte surface area $\alpha = 5.0 \times 10^5$ m^2 m^{-3}. The cathode CL is the lower part and the anode CL the upper [46].

the larger is the membrane water diffusion coefficient. Hence a better humidified membrane should yield a lower (or more negative) net drag coefficient compared to a dryer membrane under otherwise similar conditions. We assumed a constant EOD of unity under all conditions; the results will indicate that $\lambda > 3$ for all conditions investigated which verifies this simplification [2].

During this study it soon emerged that the specific surface area α of the electrolyte in the CL plays a predominant role on the overall water transport. As this value is very difficult to determine in practice and it can be easily modified simply for varying the amount of electrolyte added to the catalyst ink adjacent to the membrane, we conducted this study for three different values of α which are 5.0×10^4 m^2 m^{-3} ("low α"), 1.0×10^5 m^2 m^{-3} ("medium α"), and 5.0×10^5 m^2 m^{-3} ("high α"), respectively.

4.2. Cases without MPL

This study contains cases with and without an MPL. In the first section the MPL was left out. The overall thickness of the GDL was the same whether it contained an MPL or not.

4.2.1. Case 1

In the fully humidified case there should be only net water transport from anode to cathode because there is a near-zero RH gradient across the membrane which means that the driving force for back diffusion is low. Fig. 2a and b shows the resulting net drag coefficient and the membrane water content as function of current density for the different specified values of the specific electrolyte surface area α in the CL. The drag coefficient is fairly independent of the current density which is in agreement with experiments [20] but it varies strongly with α. The membrane water content is highest for the highest specified value of α, and this should result in a superior cell performance. Hence for these operating conditions a water uptake layer should be beneficial.

Fig. 3a and b shows the predicted membrane water content as calculated in *Domain IV* at a current density of 0.8 A cm^{-2}, and they demonstrate an additional reason why the performance should be highest for the case with high α. The water content inside the MEA exhibits a strong variation, and it is interesting to note that the anode side water content is predicted higher than the cathode side while it is common presumption that the anode side of the membrane is prone to dehydration. While the anode water content is at maximum ($\lambda \approx 13$) the cathode CL water content is a strong function of α. It will be seen below that the fundamental reason for this behavior is the variation of the net drag coefficient with α. In all cases the net transport is from anode to cathode (see Fig. 2). Even though we encounter significant liquid water saturation at the cathode CL of above 30% (see Fig. 4) the electrolyte phase is not fully hydrated, which is in contrast to the frequently assumed equilibrium between electrolyte phase and gas (liquid) phase. In all of the contour plots the results have been mirrored so that the full land area is shown in the middle (−0.5 mm to 0.5 mm) of the plot and two half-channel areas at the sides.

Finally, Fig. 4 shows that the predicted liquid water content (calculated in *Domain I)* at the cathode side is only weakly dependent on both current density and α, but it is very interesting to note that the anode side water content shows a strong dependence: while the anode always remains in the single phase at low current densities and for a low α it becomes multi-phase at a high current density and high α. Fig. 4 shows that under the latter conditions there is a significant amount of water predicted at the anode side under land. This water content of around 20% corresponds to the irreducible saturation, meaning that it is not transported by capillary action. The interface between anode GDL and channel remains dry, no liquid water enters the anode flow channel. This water will probably not impact the cell performance but it will be detected in Neutron Radiography experiments.

For the sake of completeness the relative humidity distribution inside the cell (Fig. 5a and b) and the local evaporation rates (Fig. 6a and b) are shown as well. Both are calculated at a current density at 0.8 A cm^{-2} for the low α case and the high α case, respectively. The relative humidity changes drastically at the anode side when we apply a different α. While we observe a dryer gas phase at the

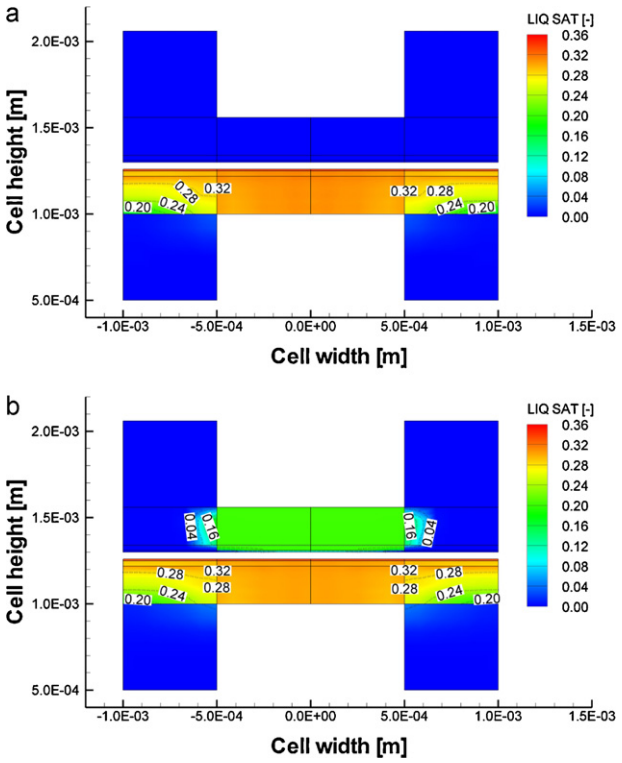

Fig. 4. (a) Predicted liquid saturation at the cathode (lower) and anode (upper) half cell for Case 1 at a current density of 0.8 A cm^{-2} and $\alpha = 5.0 \times 10^4$ m^2 m^{-3} [46]. (b) Predicted liquid saturation at the cathode (lower) and anode (upper) half cell for Case 1 at a current density of 0.8 A cm^{-2} and $\alpha = 5.0 \times 10^5$ m^2 m^{-3} [46].

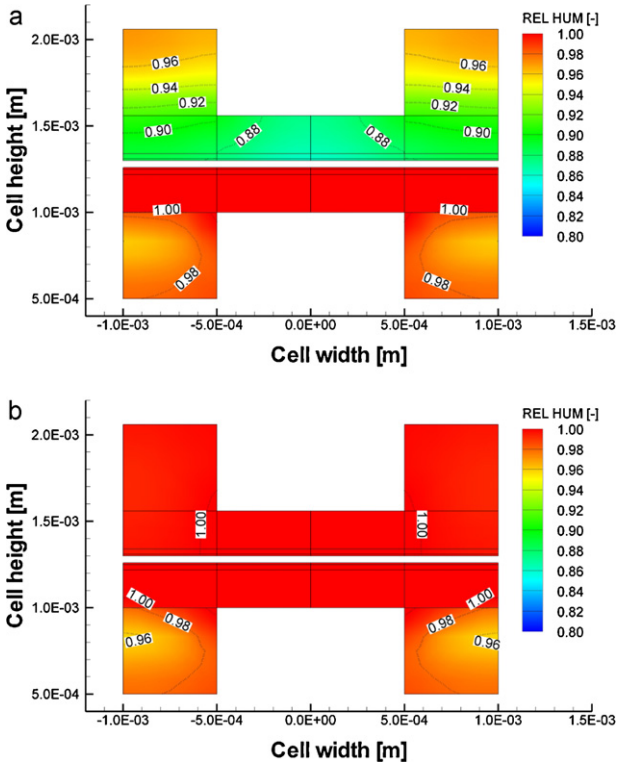

Fig. 5. (a) Predicted relative humidity distribution at the cathode (lower) and anode (upper) half cell for Case 1 at a current density of 0.8 A cm^{-2} and $\alpha = 5.0 \times 10^4$ m^2 m^{-3} [46]. (b) Predicted relative humidity distribution at the cathode (lower) and anode (upper) half cell for Case 1 at a current density of 0.8 A cm^{-2} and $\alpha = 5.0 \times 10^5$ m^2 m^{-3} [46].

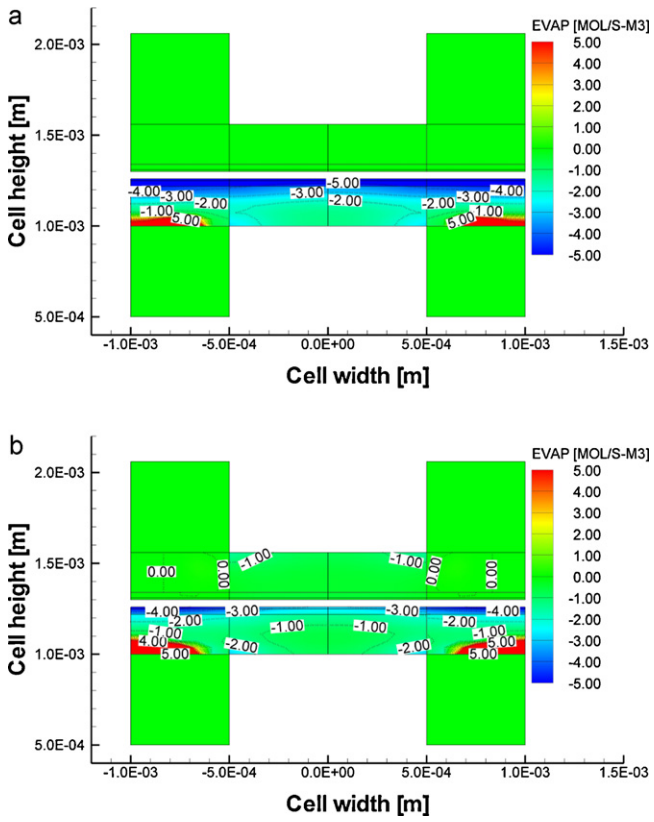

Fig. 6. (a) Predicted local rate of phase change at the cathode (lower) and anode (upper) half cell for Case 1 at a current density of 0.8 A cm^{-2} and $\alpha = 5.0 \times 10^4$ m^2 m^{-3}. (b) Predicted local rate of phase change at the cathode (lower) and anode (upper) half cell for Case 1 at a current density of 0.8 A cm^{-2} and $\alpha = 5.0 \times 10^5$ m^2 m^{-3}.

anode due to the positive drag coefficient in the case of low α the anode side remains fully humidified for high α.

Fig. 6 shows that the local evaporation rate inside the cathode porous media becomes larger and the condensation zone becomes smaller with increasing α. The condensation zone near the CL is due to the oxygen consumption, as was described by Berning and Djilali [39]. To summarize, it was observed above that an increasing α in this case means that the net drag becomes smaller, i.e. lower water transport to the cathode. The consequence of this is that removing liquid water from the cathode will be less problematic.

4.2.2. Case 2

In this case the inlet gases were partly humidified at both half cells. Due to the water production at the cathode this results in the build-up of a significant concentration gradient between anode and cathode. This concentration gradient is further increased by the EOD. Hence compared to the fully humidified case there is a stronger driving force for back diffusion, and this can even cause the overall water transport from cathode to anode, i.e. a negative net drag coefficient.

Fig. 7a shows that in this case the net drag coefficient can either be positive or negative, depending on the specific surface area of the electrolyte in the CL. A high value of α increases the back-diffusion. The net drag generally increases with current density meaning that the effect of the EOD becomes relatively stronger. Fig. 7b shows that the average water content inside the membrane is quite similar in all cases at values around $\lambda = 7$–8. A side effect of using a water uptake layer is that we can avoid the liquid regime at the cathode CL altogether, which leads to an increased limiting current density, as shown in Fig. 7c. Here we see from the average oxygen concentration that for low α the cathode CL is in the two-phase region

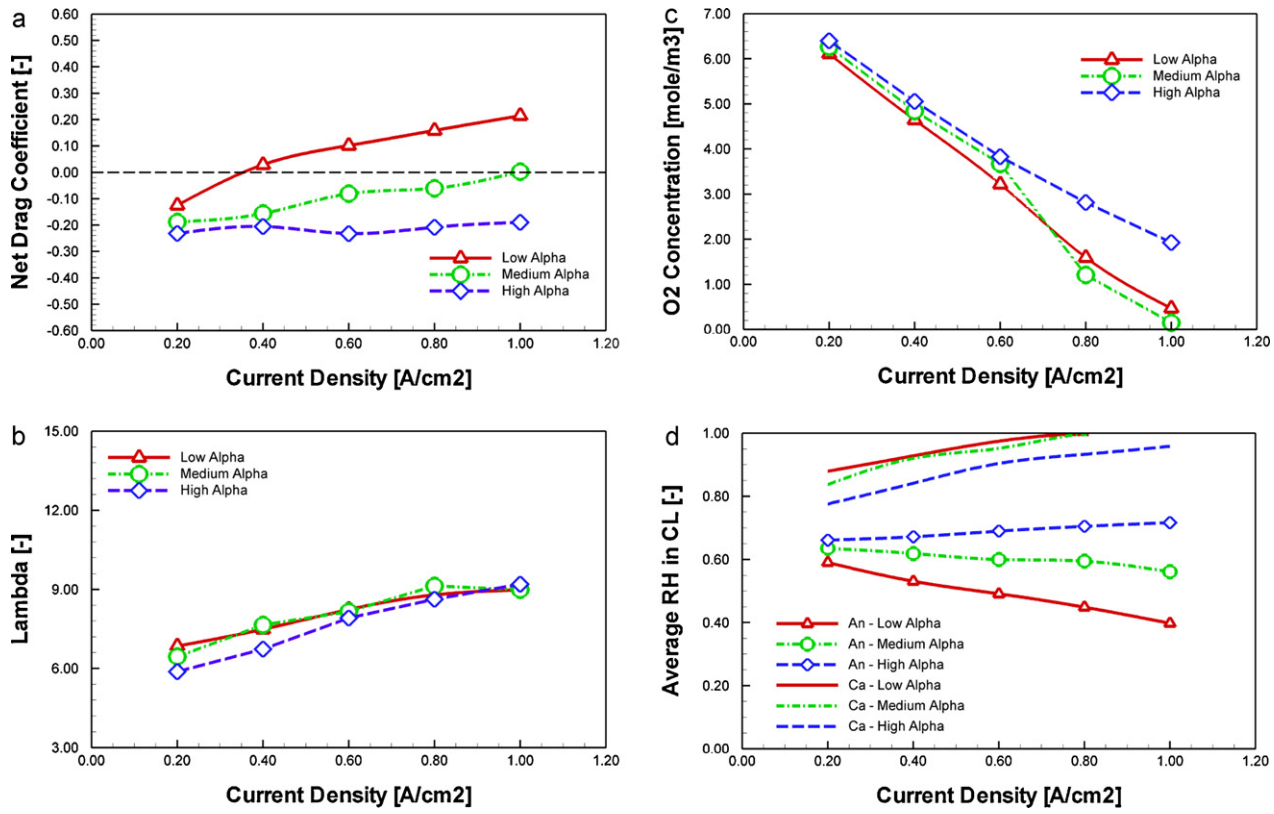

Fig. 7. (a) Predicted net drag coefficient for Case 2 as function of the specific electrolyte surface area α [46]. (b) Predicted average membrane water content λ for Case 2 as function of the specific electrolyte surface area α [46]. (c) Predicted average oxygen concentration in the CL for Case 2 as function of the specific electrolyte surface area α [46]. (d) Predicted average relative humidity in the CL for Case 2 as function of the specific electrolyte surface area α.

for all current densities and in the single phase region for high α, while it undergoes a transition between 0.6 A cm^{-2} and 0.8 A cm^{-2} for medium α. Fig. 7d summarizes the average relative humidity in anode and cathode CL as function of α. A water uptake layer significantly lowers the humidification gap between anode and cathode and can prevent or reduce cathode flooding, as was observed above. Moreover, it may help to "recycle" water when anode and cathode operate in counter-flow and the gases enter at a fairly low RH as was proposed by Büchi and Srinivasan [40].

From Fig. 7a it can also be observed that at a current density of 1.0 A cm^{-2} the net drag is positive for low α and negative for high α. Fig. 8a and b shows the detailed calculated distribution of the electrolyte water content λ for these cases. In case of a positive net drag (Fig. 8a) the concentration gradient of water inside the membrane points from anode to cathode, i.e. the cathode side is dryer than the anode side, while for a negative net drag the concentration gradient points from cathode to anode. This is a direct consequence of Eq. (8), which describes the water transport in the electrolyte membrane as pure diffusion. This implies that it depends entirely on the net drag of water through the membrane, which side will become dryer. While it is common perception that the membrane dries out on the anode side (because the gas phase here is dryer), these results indicate that it is just as likely that the cathode side membrane may be the dry side. Although this finding is a direct consequence of Eq. (8), it does not agree with experiments conducted by Büchi and Scherer who found that it is always the anode side that becomes dry [41].

The cathode side of the fuel cell has much larger mass transport losses than the anode side, and as a consequence the local current density moves away from the CL/membrane interface with increasing current density [29]. A drier electrolyte phase inside the cathode CL means that there will be increased protonic loss here and this should be prevented in order to optimize the cell performance. Consequently, operating conditions that cause a high net drag from anode to cathode should be avoided. A water uptake layer may also prevent such condition.

Finally, Fig. 9a shows the predicted liquid saturation inside the cell at a current density of 1.0 A cm^{-2} for a low value of α. This water can be completely removed by increasing α and hence reversing the net drag coefficient. There is no liquid water under the same conditions for high α (not shown), and the predicted RH distribution stays just below 100%, as shown in Fig. 9b. As was observed above,

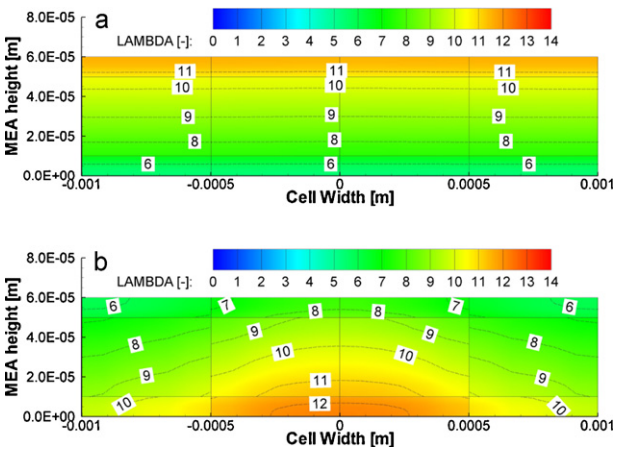

Fig. 8. (a) Predicted membrane water content λ for Case 2 at a current density of 1.0 A cm^{-2} for the low specific electrolyte surface area α [46]. (b) Predicted membrane water content λ for Case 2 at a current density of 1.0 A cm^{-2} for the high specific electrolyte surface area α [46].

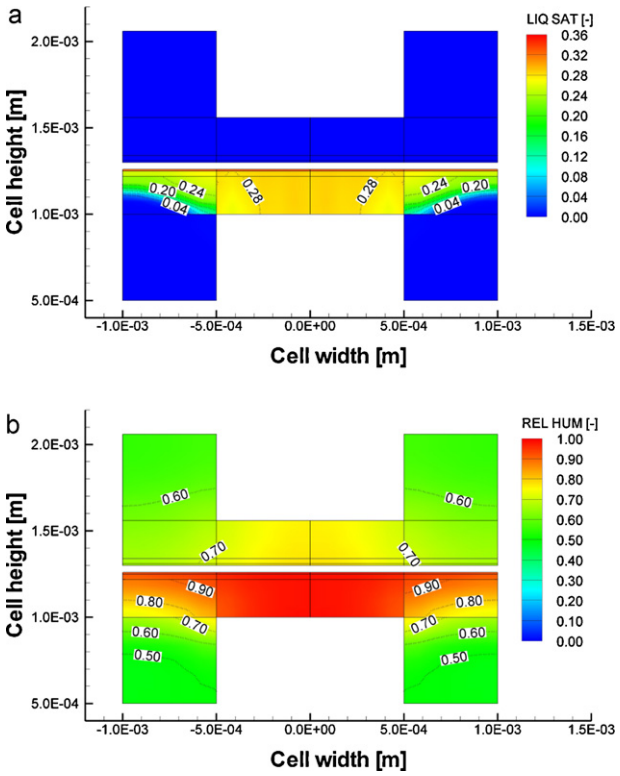

Fig. 9. (a) Predicted liquid saturation at the cathode (lower) and anode (upper) half cell for Case 2 at a current density of 1.0 A cm^{-2} for $\alpha = 5.0 \times 10^4$ m^2 m^{-3} [46]. (b) Predicted RH distribution at the cathode (lower) and anode (upper) half cell for Case 2 at a current density of 1.0 A cm^{-2} for $\alpha = 5.0 \times 10^5$ m^2 m^{-3} [46].

this significantly increases the predicted limiting current density from around 1.0 A cm^{-2} at a lower α to over 1.2 A cm^{-2} at high α.

4.2.3. Case 3

In order to simplify system cost and complexity it is desirable to operate a low temperature PEMFC without external humidification. However, it is commonly believed that this leads to membrane dehydration and consequently to a low cell performance. In early works Büchi and Srinivasan experimentally investigated the possibility to operate the fuel cell without external humidification [40]. Later, Büchi and Scherer built fuel cells with varying membrane thickness and found that the limiting current density and overall membrane resistance is strongly dependent on the membrane thickness and hence on the ability of the membrane to transport water to the anode via back diffusion [41].

Case 3 was carried out for the case of dry incoming reactant gases. We assume that such a case can only function with a negative net drag coefficient, as otherwise there will be no water at the anode side to sustain the EOD. Hence, the limiting current density is reached when the net drag approaches zero. Fig. 10 shows the predicted development of the net drag coefficient. The drag coefficient is in the negative regime and approaches zero with increasing current density for all cases. In case of a high α the net drag remains negative throughout the entire current density range investigated.

If we work from the hypothesis that the limiting current density is reached when the net drag becomes zero, then for the low α case the overall cell current is limited for the water transport through the membrane at 0.5 A cm^{-2} and for the medium α case at around 1.0 A cm^{-2}. Applying a water uptake layer may mean that the limiting current density is not determined by the ability of the cell to shed water to the anode. The predicted membrane water content is shown in Fig. 10b. Despite the fact that the gases enter the cell completely dry the membrane water level is around $\lambda \approx 5$ and

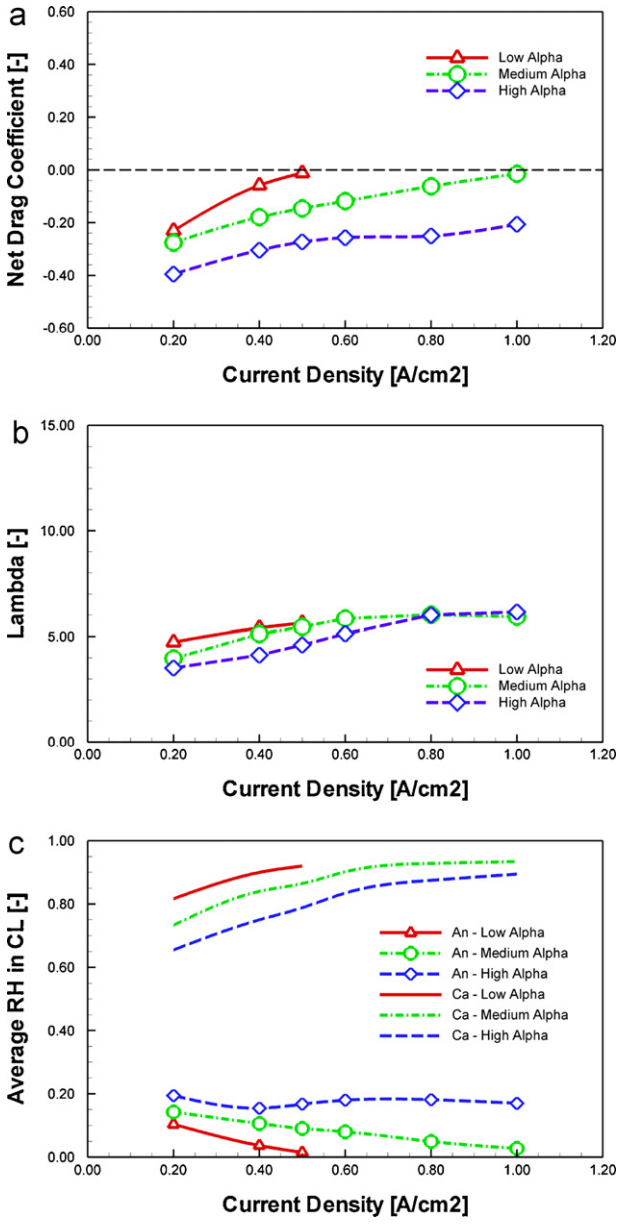

Fig. 10. (a) Predicted net drag coefficient for Case 3 as function of the specific electrolyte surface area α [46]. (b) Predicted average membrane water content λ for Case 3 as function of the specific electrolyte surface area α [46]. (c) Predicted average relative humidity inside the CL for Case 3 as function of the specific electrolyte surface area α.

varies little with current density. There is only a very small variation in λ predicted as function of the specific surface area. While a partly dehydrated membrane will lead to a worse cell performance due to high ohmic losses inside the membrane it may be still worth considering for some applications due to the significant reduction in system complexity and cost (no humidifier required). Because the net drag coefficient is always negative in this case this means that the electrolyte phase in the cathode CL is better humidified than in the anode CL. Moreover there are no liquid water problems expected at this set-up, but this may change for realistic stoichiometric flow ratios. Fig. 11a and b shows the predicted membrane water content for the medium α case and the high α case at a current density of 1.0 A cm^{-2}, where the cathode CL is significantly better humidified for the high α case due to the high back diffusion while there is again a near-zero gradient for the medium α case.

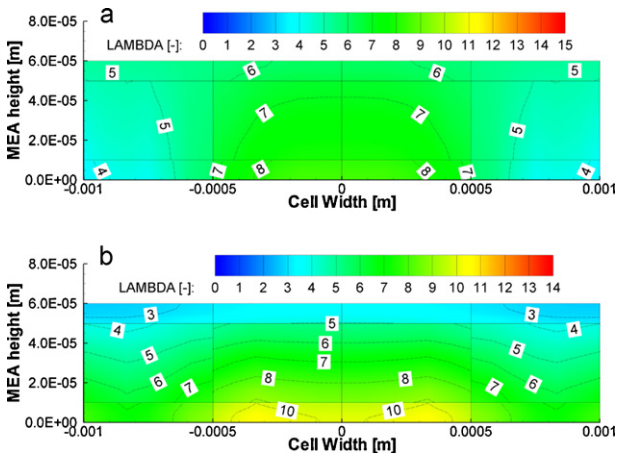

Fig. 11. (a) Predicted average membrane water content λ for Case 3 at a current density of 1.0 A cm^{-2} and a medium specific electrolyte surface area α [46]. (b) Predicted average membrane water content λ for Case 3 at a current density of 1.0 A cm^{-2} and a high specific electrolyte surface area α [46].

We can conclude from this that a high specific surface area of electrolyte may yield acceptable currents when operating the cell under dry inlet conditions. It is advisable to conduct experiments under these operating conditions using different MEAs with varying electrolyte loading in the CL ink in order to verify these findings.

4.2.4. Case 4

The fourth case was performed with a fully humidified anode (100% RH) and completely dry air entering the cathode (0% RH). This was also done in order to demonstrate the numerical robustness of our model. In addition, there are publications of experimental works that make this case suitable for verification.

In general the results of this case are quite comparable with Case 1, where both anode and cathode were fed with fully humidified gases. Fig. 12a shows that the resulting drag coefficient was predicted positive for all value of α investigated, but it decreased with current density, which means that relatively speaking the effect of back diffusion becomes stronger with current density. This in turn is in part due to the better humidified membrane (see Fig. 12b), which leads to a higher diffusion coefficient, and in part due to an increase in RH at the cathode CL due to higher water production, which increases the driving force for diffusion. A detailed analysis of the results revealed that all cases were in the single phase regime at both anode and cathode and the anode RH inside the CL was always higher than the cathode RH. Note again that the net water transport can be positive due to EOD even when the RH inside the cathode CL is higher than the anode RH. The predicted membrane water content increases with current density from values around $\lambda \approx 9$ to around $\lambda \approx 12$. As the net water transport was positive throughout this case the cathode side membrane was predicted dryer than the anode side membrane.

Experimental verification of some of these findings can be found in publications by Watanabe et al. [42] who placed Platinum wires inside a Nafion membrane to measure the resistance during fuel cell operation. They found that the membrane resistance decreased with increasing current density under similar operating conditions (fully humidified anode, dry cathode). We can confirm this trend in our simulations. On the other hand Büchi and Scherer [43] measured the membrane resistance of Nafion 117 by pulse response, which however included the electrolyte resistance in the CL's as well. They used similar experimental conditions and found that the overall resistance increased with current density which appeared to contradict the results of Watanabe et al. [42]. To clarify this we conducted simulations using a thicker (180 μm) membrane that

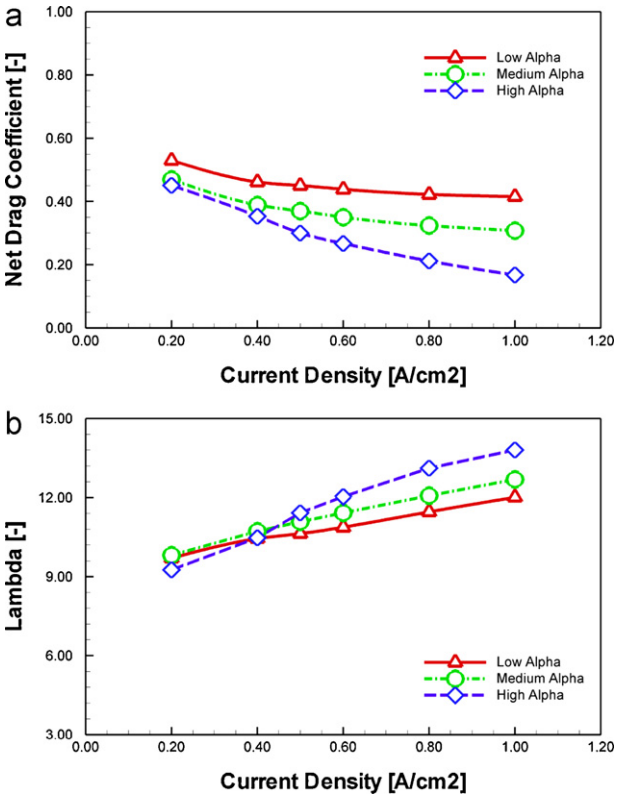

Fig. 12. (a) Predicted net drag coefficient for Case 4 as function of the specific electrolyte surface area α [46]. (b) Predicted average membrane water content λ for Case 4 as function of the specific electrolyte surface area α [46].

resembled Nafion 117. It should be kept in mind that under such operating conditions with a fully humidified anode and a dry cathode inlet gas the effective drag will invariably be positive, which means that the cathode CL will be dryer than the anode CL. Fig. 13 shows the calculated membrane water content as well as the average water content in the cathode catalyst layer (CCL). While the predicted membrane water content increases with current density as was also measured by Watanabe et al. [42] the CCL electrolyte water content decreases with low and medium α. Along with the fact that the protons have to migrate deeper into the catalyst layer with increasing current density (due to mass transport limitations on the oxygen side) this may lead to a non-linear increase in protonic resistance as observed by Büchi and Scherer. Hence this model

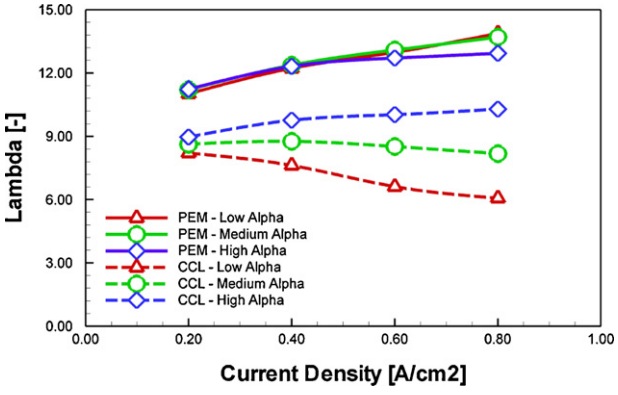

Fig. 13. Predicted average membrane and cathode CL water content λ for a Nafion 117 membrane and inlet RH of 100%/0% (A/C) as function of the specific electrolyte surface area α.

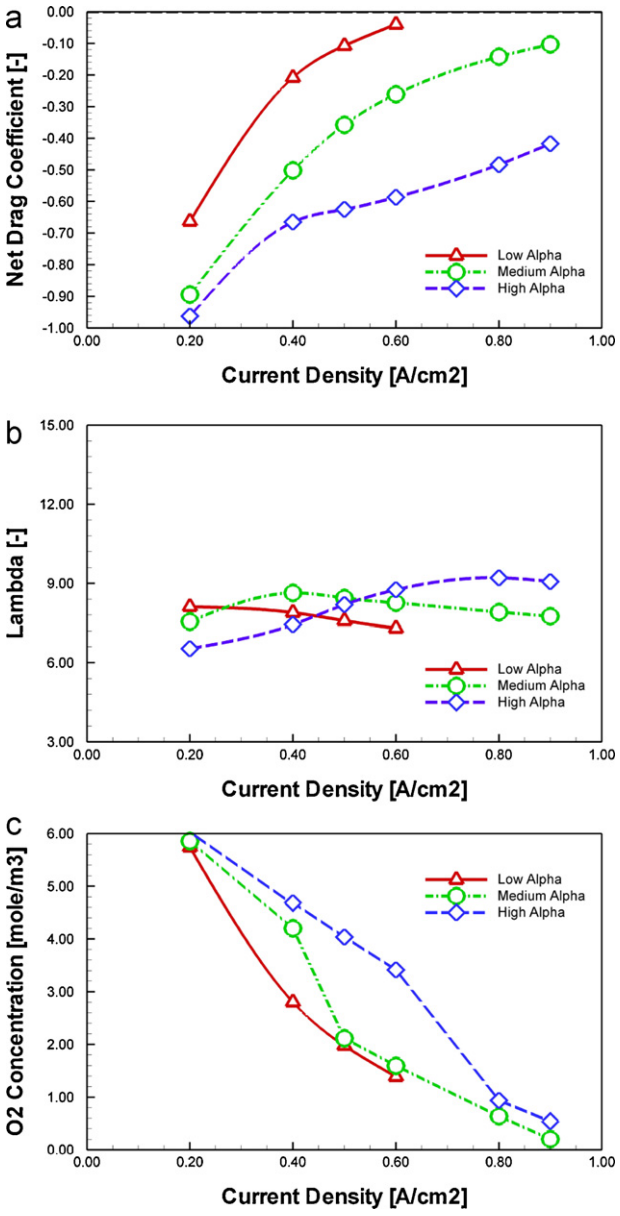

Fig. 14. (a) Predicted net drag coefficient for Case 5 as function of the specific electrolyte surface area α [46]. (b) Predicted average membrane water content λ for Case 5 as function of the specific electrolyte surface area α [46]. (c) Predicted average oxygen concentration in the cathode CL for Case 5 as function of the specific electrolyte surface area α [46].

has helped to explain this apparent contradiction in these two experiments.

4.2.5. Case 5

In Case 5 the cathode was fully humidified and the hydrogen entered completely dry. Again the hypothesis was that this cell could only function as long as the net drag remained negative. This case is somewhat comparable to Case 3, where completely dry gases entered on both sides. As could be expected, the resulting net drag coefficient is far in the negative regime (see Fig. 14a). The limiting current density for the low α case is around 0.6–0.7 A cm^{-2} while for the medium α and high α case the maximum current density is not limited by the capability to shed water to the anode. Fig. 14b shows that the average membrane water content λ is yet again fairly stable in all cases at around 7–9, and Fig. 14c suggests from the oxygen concentrations in the CL that up to a current density of

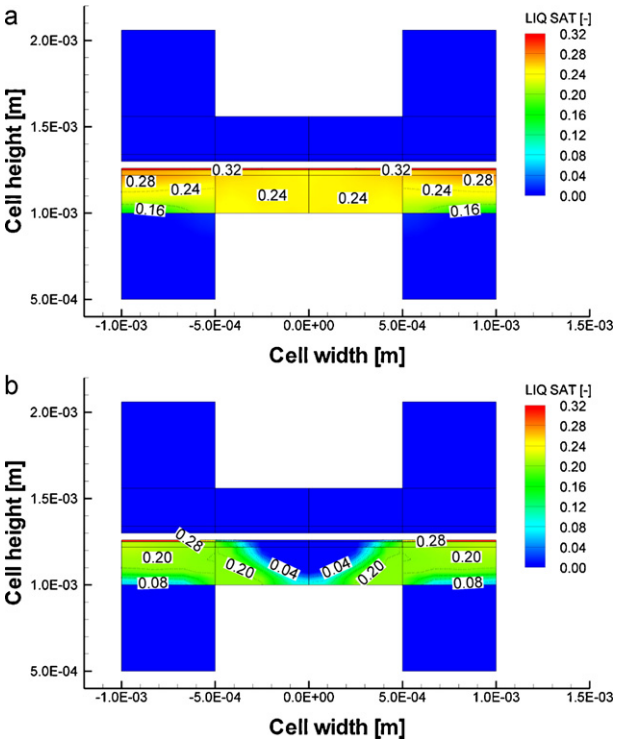

Fig. 15. (a) Predicted liquid saturation at the cathode (lower) and anode (upper) half cell for Case 5 at a current density of 0.8 A cm^{-2} for $\alpha = 1.0 \times 10^5$ m^2 m^{-3} (medium α) [46]. (b) Predicted liquid saturation at the cathode (lower) and anode (upper) half cell for Case 5 at a current density of 0.8 A cm^{-2} for $\alpha = 5.0 \times 10^5$ m^2 m^{-3} (high α).

0.4 A cm^{-2} the cathode CL is in the single phase regime for medium α, while for high α it is in the single phase regime up to a current of 0.6 A cm^{-2}.

Fig. 15a and b shows the liquid saturation for two chosen cases, one at medium α and one for high α. In the high α case the cathode flooding is significantly less pronounced, and it can also be seen that our code is capable of predicting both a "dry-to-wet" and "wet-to-dry" transition. The distribution of the membrane water content for these cases is shown in Fig. 16a and b. Because the net drag in the high α case was much more negative (from cathode to anode) the resulting gradient in water content across the membrane is very high, leading to a well humidified cathode CL. In the medium α case the cathode CL was completely in the wet regime, as can be seen in

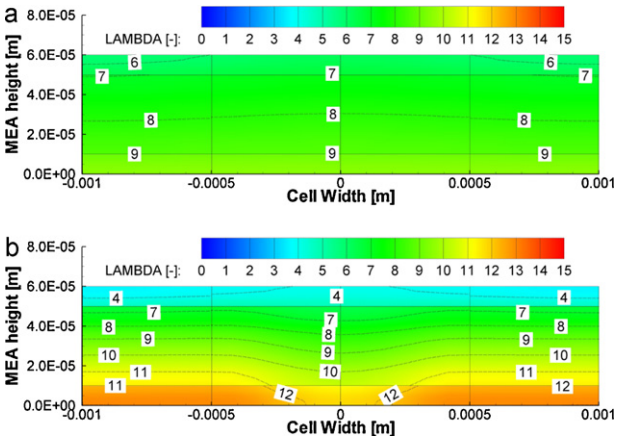

Fig. 16. (a) Predicted membrane water content λ for Case 5 at a current density of 0.8 A cm^{-2} and a medium specific electrolyte surface area α. (b) Predicted membrane water content λ for Case 5 at a current density of 0.8 A cm^{-2} and a high specific electrolyte surface area α.

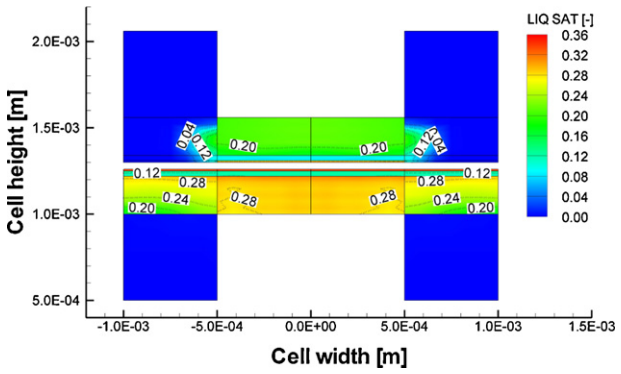

Fig. 17. Predicted liquid saturation at the cathode (lower) and anode (upper) half cell for Case 1 at a current density of 0.8 A cm^{-2} for $\alpha = 5.0 \times 10^5$ m^2 m^{-3} when an MPL was included at anode and cathode side.

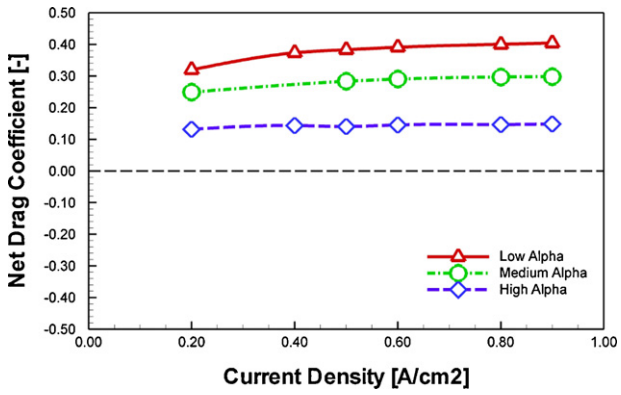

Fig. 18. Predicted net drag coefficient for Case 1 as function of the specific electrolyte surface area α when an MPL was included.

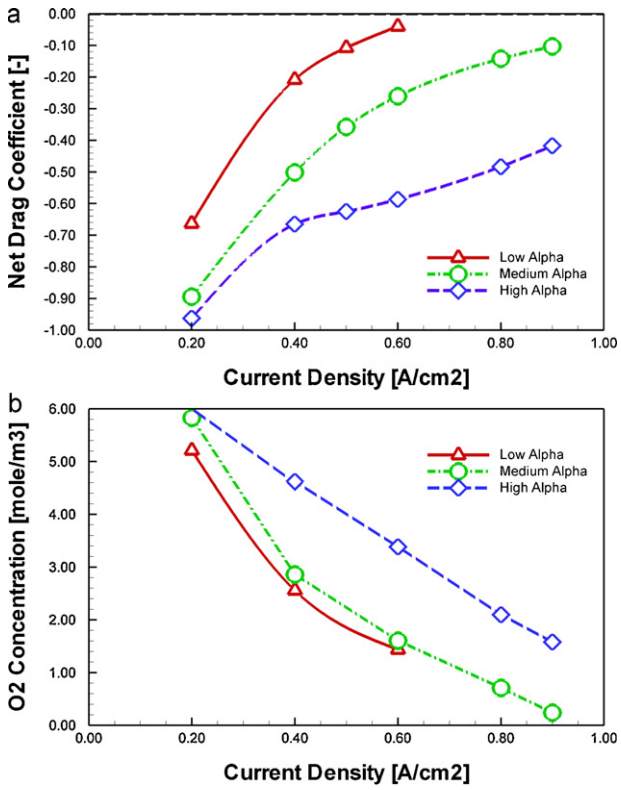

Fig. 19. (a) Predicted net drag coefficient for Case 5 as function of the specific electrolyte surface area α when an MPL was included. (b) Predicted average oxygen concentration in the cathode CL for Case 5 as function of the specific electrolyte surface area α when an MPL was included.

Fig. 15a, but the resulting water content in the electrolyte was only around 9–10, hence far from its equilibrium value (see Fig. 16a).

4.3. Cases with MPL

When an MPL was included it was 30 μm thick. As listed in Table 1 the MPL was modeled having a lower permeability, a higher contact angle by comparison to the GDL and CL and a lower irreducible saturation while the porosity was assumed to be the same as for the GDL. The tortuosity was also increased for the MPL. Note that in a CFD model the porosity predominantly plays a role in transient simulations; it cancels out of the equations in steady state simulations (except for the species diffusion coefficients). The above changes to the material properties mean that the MPL is more hydrophobic and less permeable than the GDL, and it provides a larger diffusion resistance due to the higher tortuosity. These changed material parameters have also been applied in a similar manner by Pasaogullari and Wang [44].

While all cases as above were conducted in the same detail with MPL we can summarize the results by stating that the predicted impact of the MPL on the water balance and membrane water content was very small for all cases. In most cases there appeared to be no difference at all in the predicted results whether an MPL was included or not.

Fig. 17 shows the predicted liquid water saturation for Case 1 at a current density of 0.8 A cm^{-2} for a high α when an MPL is included. This compares to Fig. 4b, where no MPL was included. We can clearly see the predicted saturation jumps between CL and MPL and between MPL and GDL [7]. As was discussed by Nam and Kaviany [27] these jumps arise out of the condition that the liquid phase pressure (capillary pressure) is continuous over the interfaces, but the saturation versus capillary pressure functions vary for each layer. Pasaogullari and Wang had similar findings [44]. However, when looking at the predicted net water drag for this case including an MPL we can see that there is almost no effect predicted. Fig. 18 shows very similar results to Fig. 2a.

The strongest effect of the MPL was found in Case 5, where the cathode gas enters fully humidified and the anode gas enters completely dry. While the predicted water balance is very similar with and without MPL (compare Figs. 19a and 14a) addition of the MPL leads to a higher limiting current density in the case of high α (compare Figs. 19b and 14c). This is owing to the fact that significantly less liquid water is predicted at the cathode side at elevated current densities (compare Figs. 20 and 15b).

Overall it must be stated that in general the addition of an MPL in our model by modifying material parameters such as apparent contact angle (increased hydrophobicity), permeability (increased pressure drop), irreducible saturation (smaller fraction

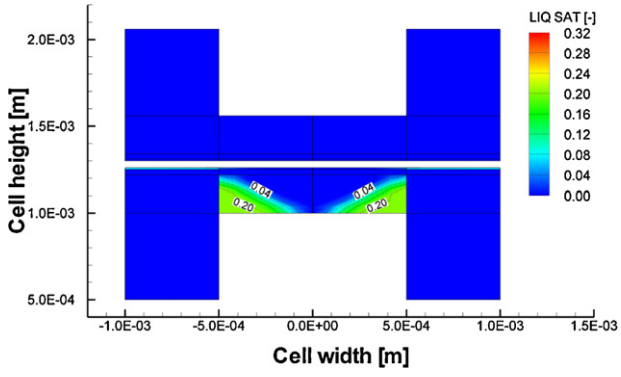

Fig. 20. Predicted liquid saturation at the cathode (lower) and anode (upper) half cell for Case 5 at a current density of 0.8 A cm^{-2} for $\alpha = 5.0 \times 10^5$ m^2 m^{-3} (high α) when an MPL was included.

of hydrophilic pores) and tortuosity (increased diffusion resistance) did not noticeably affect the water balance or membrane water content. This is in accord with experimental work conducted by Karan et al. [22].

5. Conclusions

We presented a CFD model of a PEMFC that has novel features and utilizes the multifluid approach. The computational domain was split up into five subdomains which greatly improved convergence behavior at the cost of having a slightly higher number of computational cells. A study was carried out under quasi two-dimensional operating conditions (short active area, high stoichiometric flow ratios) in order to gain fundamental understanding of the transport processes involved. The following conclusions can be drawn from this study:

- The overall water balance can depend strongly on the specific surface area of electrolyte in the catalyst layers because for thin membranes the net water transport might be limited by sorption/desorption kinetics. This can potentially be verified experimentally by varying the electrolyte loading close to the CL/membrane interface.
- The micro-porous layer was not found to have a notable impact on the water content or water transport across the membrane. In accordance with previous studies it was found that the water saturation level inside the MPL is lower than inside the GDL, but this does not impact the predicted saturation level inside the CL, nor does it affect the net water balance. More work is needed on fundamentally understanding the role of the MPL in addition to its beneficial effect due to decreased electronic resistance between the GDL substrate and the CL [45].
- The net drag coefficient alone defines which side of the electrolyte membrane becomes dehydrated. This was concluded from fundamental considerations by looking at the transport equation for water inside the membrane which reduces to a diffusion equation with no source terms. Consequently, a high positive drag (from anode to cathode) means that there is a large concentration drop of water inside the membrane from anode to cathode, i.e. the cathode becomes dry. This state should be avoided as then the electrolyte phase in the cathode CL is predicted dry, too, which means that we encounter high protonic losses. At high current densities the local current generation in the CL moves away from the membrane due to mass transport limitations which further amplifies the detrimental effect of a dry electrolyte phase.
- If we start from the hypothesis that the cell can only operate when the anode side is prevented from drying out we may be able to operate the cell under dry anode inlet conditions by adjusting the specific surface area of the electrolyte in the CL.
- Even when operating the cell under completely dry conditions the membrane water content was predicted to be 4–5, hence far from being completely dry.
- On the other hand the membrane water content was not always at its maximum when both gases enter the cell fully humidified (Case 1). A high net water drag means that the cathode side of the membrane dries out.
- Anode liquid water was found only at high current densities and for high values of the specific surface area of the electrolyte in the CL. This water was located under land only and was not predicted to reach the GDL/channel interface.
- Hydraulic permeation of water through the PEM was found to be at least two orders of magnitude smaller than diffusion/EOD.

Most of these findings can be verified by conducting suitable experiments, which will be the focus of our future work.

Acknowledgments

This work was carried out under the Danish Energy Program, Grant # 33032-0145. During part of it TB stayed at the Canadian Research Council, Institute of Fuel Cell Innovation (IFCI) in Vancouver, BC. He would like to thank Dr. Simon Liu and Dr. Qianpu Wang for their kind support.

References

[1] T.A. Zawodzinski, J. Davey, J. Valerio, S. Gottesfeld, Electrochim. Acta 40 (1995) 297–302.
[2] X. Ye, C.-Y. Wang, J. Electrochem. Soc. 154 (2007) B676–B682.
[3] T.V. Nguyen, R.E. White, J. Electrochem. Soc. 140 (1993) 2178–2186.
[4] T.E. Springer, T.A. Zawodzinski, S. Gottesfeld, J. Electrochem. Soc. 138 (1991) 2334–2342.
[5] C.W. Monroe, T. Romero, W. Merida, M. Eikerling, J. Membr. Sci. 324 (2008) 1–6.
[6] S. Ge, X. Li, B. Yi, I. Hsing, J. Electrochem. Soc. 152 (2005) A1149–A1157.
[7] T. Berning, M. Odgaard, S. Kær, J. Electrochem. Soc. 156 (2009) B1301.
[8] T. Berning, M. Odgaard, S. Kær, J. Power Sources 195 (2010) 4842–4852.
[9] O.E. Kongstein, T. Berning, B. Børresen, F. Seland, R. Tunold, Energy 32 (2007) 418–422.
[10] W. Dai, H. Wang, X.-Z. Yuan, J.J. Martin, D. Yang, J. Qiao, et al., Int. J. Hydrogen Energy 34 (2009) 9461–9478.
[11] J.J. Baschuk, X. Li, Int. J. Hydrogen Energy (2009).
[12] D.M. Bernardi, J. Electrochem. Soc. 137 (1990) 3344–3350.
[13] P. Berg, K. Promislow, J. St. Pierre, J. Stumper, B. Wetton, J. Electrochem. Soc. 151 (2004) A341–A353.
[14] W.-K. Lee, S. Shimpalee, J.W. Van Zee, J. Electrochem. Soc. 150 (2003) A341–A348.
[15] C. Siegel, Energy 33 (2008) 1331–1352.
[16] G. Luo, H. Ju, C.-Y. Wang, J. Electrochem. Soc. 154 (2007) B316–B321.
[17] H. Wu, X. Li, P. Berg, Electrochim. Acta 54 (2009) 6913–6927.
[18] Q. Ye, T.V. Nguyen, J. Electrochem. Soc. 154 (2007) B1242–B1251.
[19] F. Liu, G. Lu, C.-Y. Wang, J. Membr. Sci. 287 (2007) 126–131.
[20] G.J.M. Janssen, M.L.J. Overvelde, J. Power Sources 101 (2001) 117–125.
[21] Y. Cai, J. Hu, H. Ma, B. Yi, H. Zhang, Electrochim. Acta 51 (2006) 6361–6366.
[22] K. Karan, H. Atiyeh, A. Phoenix, E. Halliop, J.G. Pharoah, B. Peppley, Electrochem. Solid-State Lett. 10 (2007) B34–B38.
[23] Q. Yan, H. Toghiani, J. Wu, J. Power Sources 158 (2006) 316–325.
[24] X. Ye, C.-Y. Wang, J. Electrochem. Soc. 154 (2007) B683–B686.
[25] M.C. Leverett, Trans. AIME 142 (1976) 152.
[26] K.S. Udell, Int. J. Heat Mass Transfer 28 (1985) 485–495.
[27] J.H. Nam, M. Kaviany, Int. J. Heat Mass Transfer 46 (2003) 4595–4611.
[28] V. Gurau, T.A. Zawodzinski, J.A. Mann, J. Fuel Cell Sci. Technol. 5 (2008) 021009.
[29] M. Bang, Modeling of Diffusive Convective and Electrochemical Processes in PEM Fuel Cells, Ph.D. Dissertation, Aalborg University, 2004.
[30] G.J.M. Janssen, J. Electrochem. Soc. 148 (2001) A1313–A1323.
[31] A. Weber, J. Newman, J. Electrochem. Soc. 151 (2004) A311–A325.
[32] J. Fimrite, H. Struchtrup, N. Djilali, J. Electrochem. Soc. 152 (2005) A1804–A1814.
[33] S. Ge, B. Yi, P. Ming, J. Electrochem. Soc. 153 (2006) A1443–A1450.
[34] T.A. Zawodzinski, C. Derouin, S. Radzinski, R.J. Sherman, V.T. Smith, T.E. Springer, et al., J. Electrochem. Soc. 4 (1993) 1041–1047.
[35] D.J. Burnett, A.R. Garcia, F. Thielmann, J. Power Sources 160 (2006) 426–430.
[36] M. Eikerling, Y.L. Kharkats, A.A. Kornyshev, Y.M. Volfkovich, J. Electrochem. Soc. 145 (1997) 2684–2699.
[37] A. Weber, J. Newman, J. Electrochem. Soc. 150 (2003) A1008–A1015.
[38] M. Verbrugge, R.F. Hill, J. Electrochem. Soc. 137 (1990) 886–893.
[39] T. Berning, N. Djilali, J. Electrochem. Soc. 150 (2003) A1589–A1598.
[40] F.N. Büchi, S. Srinivasan, J. Electrochem. Soc. 144 (1997) 2767–2772.
[41] F.N. Büchi, G.G. Scherer, J. Electrochem. Soc. 148 (2001) A183–A188.
[42] M. Watanabe, I. Igarashi, H. Uchida, F. Hirasawa, J. Electroanal. Chem. 399 (1995) 239–241.
[43] F.N. Büchi, G.G. Scherer, J. Electroanal. Chem. 404 (1996) 37–43.
[44] U. Pasaogullari, C.-Y. Wang, Electrochim. Acta 49 (2004) 4359–4369.
[45] F. Seland, T. Berning, B. Børresen, R. Tunold, J. Power Sources 160 (2006) 27–36.
[46] T. Berning, M. Odgaard, S. Kær, ECS Trans. 33 (2010) 1503–1513.